Spectral broadening of a KrF laser via propagation through Xe in the negative nonlinear index regime

Zachary Epstein,[1,*] Robert H. Lehmberg,[2] and Phillip Sprangle[1,3]
[1]*University of Maryland, College Park, Maryland 20742-4111, USA*
[2]*Consultant to Naval Research Laboratory through RSI Corporation, Lanham, Maryland 20706, USA*
[3]*Plasma Physics Division, Naval Research Laboratory, Washington, DC 20375, USA*

(Received 25 April 2019; published 20 August 2019)

In inertial confinement (ICF) experiments at the NIKE laser facility, the high-power krypton fluoride (KrF) laser output beams propagate through long (∼75 m) air paths to achieve angular multiplexing, which is required because the KrF medium does not store energy for a sufficiently long time. Recent experiments and simulations have shown that, via stimulated rotational Raman scattering, this propagation can spectrally broaden the laser beam well beyond the ∼1 THz laser linewidth normally achieved by the induced spatial incoherence (ISI) technique used in NIKE. These enhanced bandwidths may be enough to suppress the laser-plasma instabilities which limit the maximum intensity that can be incident on the ICF target. In this paper we investigate an alternative technique that achieves spectral broadening by self-phase modulation in Xe gas, which has a large, negative nonlinear refractive index ∼248 nm, and thus completely avoids transverse filamentation issues. The collective, nonlinear atomic response to the chaotic, nonsteady state ISI light is modeled using a two-photon vector model, and the effect of near-resonant behavior on the spectral broadening is studied.

DOI: 10.1103/PhysRevA.100.023831

I. INTRODUCTION

A primary challenge in inertial confinement fusion is the growth of hydrodynamic instabilities and laser plasma instabilities (LPI) [1]. Increasing the laser spectral bandwidth can be an effective way of reducing the growth rates of LPI instabilities [2]. Recent experiments on the NIKE KrF laser, which uses a 75 m propagation bay for beam multiplexing, have shown that stimulated rotational Raman scattering (SRRS) in the air paths can spectrally broaden the bandwidth of the chaotic, incoherent light well beyond the ∼1 THz normally allowed by NIKE's induced spatial incoherence (ISI) technique. While SRRS is small in normal NIKE operation at moderate beam intensities (∼50 MW/cm^2), these experiments generated significant SRRS by imposing an ∼150 MW/cm^2, 400 ps spike on the pulse and folding the beam to lengthen the optical air path. The amount of spectral broadening that was achieved, however, was limited to several THz. Alternatively, to propagate in an inert gas requires a large nonlinear refractive index $n_2 \sim 60 \times 10^{-19}$ cm^2/W—five times that of air—for comparable spectral broadening. Though this would mean self-filamentation for a Gaussian beam (where the nonlinear focusing power at 248 nm in air is 100 MW), the important parameter for ISI light is the power within a single coherence zone; for a 75 times diffraction limited beam, the nonlinear focusing power in air becomes ∼500 GW.

For linearly polarized light, there exists a two-photon resonance in atomic xenon (Xe) at 249.6 nm, which has been discussed in the literature [3,4]. As a result of this resonance, Xe has a large, negative nonlinear index n_2 at the 248.4 nm KrF laser wavelength whose doubled frequency lies only 11.9 THz above the resonance; see Figs. 1 and 2. Hence propagation through Xe gas has the potential to substantially increase the spectral bandwidth of the KrF laser without the problem of self-filamentation, which is a positive-n_2 effect. The negative nonlinear index near resonance has been observed and accurately calculated from known Xe electric dipole matrix elements for narrow-band KrF light operating under steady-state conditions [3,5].

At the NIKE facility, however, the KrF laser uses incoherent beam smoothing techniques that produce chaotic variations on a ps time scale. The resulting multi-THz spectral bandwidths of interest can thus include frequencies that are much closer to the two-photon resonance than the 11.9 THz detuning of the narrow-band KrF light. As a result, the nonlinear Kerr response can experience time delays and the upper level may become partially populated during the pulse.

In this paper, we model the nonlinear response of Xe gas to chaotic non-steady-state, near-resonance light using a two-photon vector model. Although this model includes small collisional damping coefficients, they play a negligible role in spectral broadening at Xe pressures up to at least 200 mbar. Earlier work on two-photon vector models can be found in Refs. [6,7].

At 200 mbar, nonlinear refraction and two-photon absorption due to the small (0.02%) dimerization of the Xe molecules are expected to be minimal but further investigation may be needed; see Refs. [3,8]. The dimer density scales quadratically with the xenon pressure p to give an estimated two-photon attenuation coefficient [3]: $\kappa_{Xe_2}(\mathrm{m}^{-1}) \sim 0.8 \times 10^{-2}(p/1000)^2 I(\mathrm{GW/cm}^2)$. At $p = 200$ mbar and the

*zbe@umd.edu

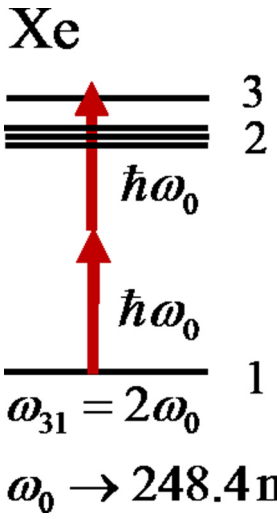

FIG. 1. Nonlinear optical response of Xe near its two-photon $5p^6 \rightarrow 6p[1/2]_0$ resonance is that of a three-level system with multiple intermediate states $|2\rangle$ and allowed electronic transitions from $|1\rangle \rightarrow |2\rangle$ and $|2\rangle \rightarrow |3\rangle$.

$0.15\,\mathrm{GW/cm^2}$ intensities typical of the simulations performed here, this gives only 0.2% attenuation over the 50 m propagation path; at higher pressures, however, dimer absorption could become an issue.

Though the laser propagation in a nonlinear medium yields spectral broadening—which is useful for the reduction of hydrodynamic and laser plasma instabilities in inertial confinement fusion—the propagation also results in far-field broadening. The consequent degradation of the laser beam profile is studied.

A detailed overview of the NIKE laser facility and its KrF laser can be found in Ref. [2]. The NIKE laser facility uses echelon-free induced spatial incoherence (ISI) to produce a laser beam that is spatially and temporally incoherent [9,10]. The beam's speckle fluctuations occur over rapid (picosecond) time scales such that they average out over hydrodynamic time scales to yield a spatially and temporally uniform illumination. This, in turn, minimizes the hydrodynamic instabilities that would otherwise be strongly seeded by laser beam spatial nonuniformities.

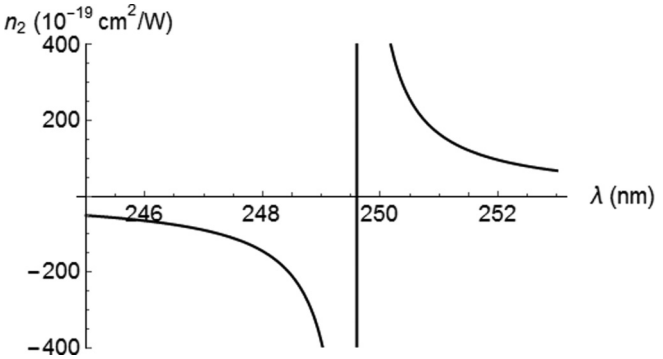

FIG. 2. Wavelength dependence of the nonlinear refractive index n_2 of 200 mbar Xe in the regime of the two-photon resonance. The curve is continuous but extends beyond the range shown here.

In Sec. II, we present the nonlinear Schrödinger equation that is used to model laser propagation through a nonlinear medium, discuss how to model the directed spatially and temporally incoherent KrF radiation, and derive a model for the nonlinear response of the Xe gas. In Secs. III and IV, respectively, we describe the numerical techniques and present simulation results. In Sec. V, we discuss the results and propose a new direction for the inertial confinement fusion experiments at the NIKE laser facility. In Sec. VI, we summarize our results.

II. MODEL

A. Laser pulse propagation: Generalized nonlinear Schrödinger equation

The electric field, in the absence of free charges, is given by the wave equation with a nonlinear source term, i.e.,

$$\nabla^2 E(\mathbf{r},t) = (\partial/\partial t)^2 E(\mathbf{r},t)/c^2 + \mu_0(\partial/\partial t)^2[P_L(\mathbf{r},t) + P_{NL}(\mathbf{r},t)],$$

where $P_L(\mathbf{r},t)$ and $P_{NL}(\mathbf{r},t)$ are respectively the linear and nonlinear polarization of the propagation medium. The electric field is taken to be linearly polarized along the x axis and the divergence term has been neglected since the beam's spatial fluctuations occur over distances much larger than the wavelength. Because (a) the nonlinear changes in the refractive index are small relative to the linear changes in the refractive index and (b) the KrF laser's fractional bandwidth $\Delta\omega/\omega_0 \ll 1$, we can make a slowly varying envelope approximation and express the wave equation as a three-dimensional generalization of the nonlinear Schrödinger equation (NLSE) [11]. The envelope equation is given by

$$\begin{aligned}(\partial/\partial\eta)E_p(\mathbf{r},\tau) &= i\nabla_\perp^2 E_p(\mathbf{r},\tau)/2k_0 + (-i\beta_2(\partial/\partial\tau)^2 E_p(\mathbf{r},\tau)/2 + \cdots) \\ &\quad + i\left(\omega_0^2/2\varepsilon_0 c^2 k_0\right)[1 + i(\partial/\partial\tau)/\omega_0]^2 P_{NL,p}(\mathbf{r},\tau), \qquad (1)\end{aligned}$$

where $\eta = z$ and $\tau = t - z/\mathrm{v}$ are the longitudinal and temporal variables in a frame moving at the group velocity v, k_0 is the wave number at the carrier frequency $\omega_0 = 2\pi c/\lambda_0$, and β_2 is the group-velocity dispersion coefficient at ω_0. The electric field is given by $E(\mathbf{r},t) = (1/2)E_p(\mathbf{r},t)\exp(ik_0 z - i\omega_0 t) + (1/2)E_p^*(\mathbf{r},t)\exp(-ik_0 z + i\omega_0 t)$ and the nonlinear polarization field (excluding higher harmonics) is given by $P_{NL}(\mathbf{r},t) = (1/2)P_{NL,p}(\mathbf{r},t)\exp(ik_0 z - i\omega_0 t) + (1/2)P_{NL,p}^*(\mathbf{r},t)\exp(-ik_0 z + i\omega_0 t)$. The wave equation given in Eq. (1) can be solved numerically via the split-step method, see Ref. [12], and is driven by the nonlinear polarization of the Xe gas, which is derived in Sec. II C.

B. Spatial and temporal incoherence

The front end of the NIKE KrF light source is a spatially and temporally incoherent ASE (amplified spontaneous emission) oscillator, which can be represented by a collection of many independent oscillators emitting at frequencies in the range of the carrier frequency, and which are scattered throughout space in such a way that the spatial frequency distribution is roughly symmetric about zero. Numerically, this

is represented by a 3D function determined according to the average output of the ASE, which we model here as Gaussian in frequency and spatial frequency space and centered about $(\omega_0, 0, 0)$. Each amplitude A_{ω,k_x,k_y}—corresponding to the sum of a large collection of independent oscillators at (ω, k_x, k_i)—is thus a Gaussian-distributed complex random number with random phase. The amplitude squared $|A_{\omega,k_x,k_y}|^2$ is then multiplied by the incident power spectrum. The resulting function A_{ω,k_x,k_y} is Fourier transformed into time and space, resulting in the function $G(t, x, y)$. The function G has been normalized according to the power of the KrF beam and multiplied by a top-hat shaped filter function, which corresponds to the beam aperture.

The ASE light, which is modeled as a quasicollimated multimode beam, traverses an aperture whose width D is ∼75 times larger than the spatial coherence zones determined by the (k_x, k_y) angular divergence. It thus takes on the structure of a 75×75 transverse array of uncorrelated beams, each of which is mostly uncorrelated with even itself after every coherence time $\tau_c = 2\pi/\Delta\omega$, where $\Delta\omega$ is the spectral bandwidth. Each uncorrelated beam is produced by a varying number of random oscillators, so the structure can be viewed as a three-dimensional, checkered array of random Gaussian numbers with random phase labeled as $F(t, x, y)$, which when integrated over many coherence times yields a flat-top beam profile.

Nonetheless, it will suffice to model the field envelope as $E_0 \times G(t, x, y)$; see Ref. [13]. A measurement of the initial beam profile or the far-field profile can be incorporated for more accurate results.

C. Nonlinear response of Xe gas

Here we derive the nonlinear polarization of the Xe gas, which is the source term of the wave propagation equation; see Eq. (1).

1. Density-matrix equations

The electric response of the Xe atom is modeled by the Hamiltonian $\hat{H}(\mathbf{r}, t) = \hat{H}_0(\mathbf{r}, t) + \hat{V}(\mathbf{r}, t)$, where $\hat{H}_0(\mathbf{r}, t)$ represents the unperturbed atom, $\hat{V}(\mathbf{r}, t) = -\mu(\mathbf{r}) \cdot \mathbf{E}(\mathbf{r}, t) = -q\mathbf{r} \cdot \mathbf{E}(\mathbf{r}, t)$ represents the electric dipole interaction, μ is the dipole moment operator, and $E(\mathbf{r}, t) = |E_p(\mathbf{r}, t)| \cos[\phi(\mathbf{r}, t)] = (1/2)E_p(\mathbf{r}, t) \exp(ik_0 z - i\omega_0 t) + \text{c.c.}$ is the classical field associated with the KrF laser light. Although the following equations can produce a nonzero third harmonic polarization, the third harmonic electric field is neglected here. This is justified because the large phase mismatch created by dispersion and cross-phase modulation strongly suppresses the convective growth of the third-harmonic field at this far UV wavelength, which is also strongly absorbed by photoionization. The slowly varying amplitude $|E_p(\mathbf{r}, t)|$ and the phase $\phi(\mathbf{r}, t)$ are real, with the instantaneous frequency given by $\omega(t) = \dot{\phi}(t) = \omega_0 + \delta\omega(t)$, where $\omega_0 = 2\pi c/\lambda_0$ and $\lambda_0 = 248.4$ nm. If the KrF light is linearly polarized, a two-photon near resonance with the Xe $6p[1/2]0$ state at 80119 cm^{-1} (2/249.63 nm) results in a negative nonlinear refractive index around λ_0. We write the wave function as $\Psi = \sum_n c_n(\mathbf{r}, t)u_n(R)$, where $u_n(R)$ is the eigenfunction corresponding to the eigenstate $|n\rangle$ of H_0 and R is the position of the outer electron with respect to the nucleus. Although multiple odd-parity intermediate eigenstates contribute to the two-photon transition, we model a three-level system here for simplicity, where $|1\rangle$ is the $5p^6$ ground state, $|2\rangle$ represents the odd-parity intermediate states, and $|3\rangle$ is the Xe $6p[1/2]0$ two-photon near-resonant state. For the closed, three-level system, the von Neumann equation $d\rho/dt = [\hat{H}, \rho]/i\hbar$ yields the following density-matrix equations:

$$
\begin{aligned}
\partial\rho_{11}/\partial t &= i(\Omega_{12}\rho_{21} - \Omega_{21}\rho_{12}) + \Gamma_I\left(\rho_{22} - \rho_{22}^{eq}\right) \\
&\quad + R\Gamma_c\left(\rho_{33} - \rho_{33}^{eq}\right), \\
\partial\rho_{22}/\partial t &= -\Gamma_I\left(\rho_{22} - \rho_{22}^{eq}\right) + i(\Omega_{21}\rho_{12} - \Omega_{12}\rho_{21}) \\
&\quad + i(\Omega_{23}\rho_{32} - \Omega_{32}\rho_{23}) + (1 - R)\Gamma_c\left(\rho_{33} - \rho_{33}^{eq}\right), \\
\partial\rho_{33}/\partial t &= -\Gamma_c\left(\rho_{33} - \rho_{33}^{eq}\right) + i(\Omega_{32}\rho_{23} - \Omega_{23}\rho_{32}), \\
\partial\rho_{12}/\partial t &= -\gamma_N\rho_{12} + i\,\omega_{21}\rho_{12} + i\,\Omega_{12}(\rho_{22} - \rho_{11}) - i\bar{\Omega}_{32}\rho_{13}, \\
\partial\rho_{13}/\partial t &= -\gamma_c\rho_{13} + i\,\omega_{31}\rho_{13} + i\,(\Omega_{12}\rho_{23} - \Omega_{23}\rho_{12}), \\
\partial\rho_{23}/\partial t &= -\gamma_L\rho_{23} + i\,\omega_{32}\rho_{23} + i\,\Omega_{23}(\rho_{33} - \rho_{22}) + i\Omega_{21}\rho_{13},
\end{aligned}
\tag{2}
$$

where the density-matrix elements are defined as $\rho_{nm}(\mathbf{r}, t) = \langle n|\rho(\mathbf{r}, t)|m\rangle = c_m^*(\mathbf{r}, t)c_n(\mathbf{r}, t)$ and where $\omega_{mn} = \omega_m - \omega_n$. The transition frequencies are defined as $\Omega_{mn}(\mathbf{r}, t) = \langle m|\hat{\mu}|n\rangle \cdot E(\mathbf{r}, t)/\hbar = \Omega_{mn}^{+}(\mathbf{r}, t) \exp[i\phi(\mathbf{r}, t)] + \Omega_{mn}^{-}(\mathbf{r}, t) \exp[-i\phi(\mathbf{r}, t)]$, where $\Omega_{mn}^{\pm}(\mathbf{r}, t) = \mu_{mn} \cdot |E_p(\mathbf{r}, t)|/2\hbar$ varies slowly in time and space and $\pm$ is a carrier frequency marker; for linear polarization we take μ_{nm} to be real and express $\Omega_{mn}^{+}(\mathbf{r}, t) \to \Omega_{mn}(\mathbf{r}, t) = \mu_{mn}|E_p(\mathbf{r}, t)|/2\hbar$. Equation (2) applies to a general three-level system with ground state $|1\rangle$, intermediate state $|2\rangle$, and excited state $|3\rangle$. The spatial symmetry of the Hamiltonian requires that $\Omega_{nn} = 0$ for each eigenstate $|n\rangle$, and we have specified the allowed transitions to be $|1\rangle \to |2\rangle \to |3\rangle$. The dynamics of inelastic collisions and spontaneous emission in the system are general, where R satisfies $0 \leqslant R \leqslant 1$ and describes the fraction of the energy emitted from $|3\rangle$ that transfers directly to $|1\rangle$.

2. Parameters

For a 248.4 nm laser pulse propagating through an atomic Xe gas, the two-photon excited state is the Xe $6p[1/2]0$ state. For a KrF NIKE pulse, we have 600 ps short pulses and 4 ns long pulses, which yield a frequency scale 1.7 GHz and 0.3 GHz, respectively. The elastic collision rate at 200 mbar is 0.5 GHz and the radiative decay rate of the excited Xe state is 0.03 GHz; see Appendix A.

3. Separation of density-matrix elements into harmonics of the laser frequency

To simplify the notation, the spatial dependence of the field and matrix elements will be dropped here but can be reincorporated in a straightforward manner. We write each

element as the sum of components at roughly the various harmonics $0, \pm\dot{\phi}(t), \pm 2\dot{\phi}(t), \pm 3\dot{\phi}(t)$ of the laser frequency:

$$\begin{aligned}\rho_{ij} = {} & \sigma_{ij}(0) + \sigma_{ij}(-\phi)\exp(-i\phi) + \sigma_{ij}(\phi)\exp(i\phi) \\ & + \sigma_{ij}(-2\phi)\exp(-2i\phi) + \sigma_{ij}(2\phi)\exp(2i\phi) \\ & + \sigma_{ij}(-3\phi)\exp(-3i\phi) + \sigma_{ij}(3\phi)\exp(3i\phi),\end{aligned}$$

where $\sigma_{ij}(-s\phi) = [\sigma_{ji}(s\phi)]^*$. The density-matrix equations are then rewritten according to Eq. (A1) for integer $s \in (-3, -2, \ldots, 3)$. We calculate the full nonlinear response to the first-harmonic field here, but will ultimately only include the first-harmonic polarization component in the analysis.

4. Two-photon vector model

For an ISI beam with temporal fluctuations that are much longer than the time scale associated with the detuning, e.g., $2\pi/\Delta \sim 0.2$ ps, where $\Delta = (2\omega_0 - \omega_{31})/2$, the off-diagonal density-matrix elements are only driven significantly near the various harmonics of the laser frequency; see Appendix A and Eq. (A3). In the case where damping terms can be neglected, we define a real vector $r = (r_1, r_2, r_3)$ according to $r_1 = \sigma_{13}(2\phi) + [\sigma_{13}(2\phi)]^*$, $r_2 = i(\sigma_{13}(2\phi) - [\sigma_{13}(2\phi)]^*)$, $r_3 = \sigma_{33}(0\phi) - \sigma_{11}(0\phi)$, and obtain the familiar (see Refs. [6,7]) two-photon vector model shown below [see Eqs. (9)–(11) for the formulation that is used for our simulations]:

$$\begin{aligned}\dot{r}_1 &= -\gamma_3 r_2, \\ \dot{r}_2 &= \gamma_3 r_1 - \gamma_1[r_3 + O(\Delta/\omega_0)] \approx \gamma_3 r_1 - \gamma_1 r_3, \\ \dot{r}_3 &= \gamma_1 r_2,\end{aligned} \tag{3}$$

where

$$\begin{aligned}\gamma_1 &= \Omega_{12}\Omega_{23}\left(\frac{1}{\omega_{21} - \dot{\phi}} - \frac{1}{\omega_{32} - \dot{\phi}}\right) \approx \frac{2\,\Omega_{12}\Omega_{23}}{\omega_{21} - \dot{\phi}} \\ &= \left(\frac{\mu_{12}\mu_{23}|E_p|^2}{2\hbar^2(\omega_{21} - \dot{\phi})}\right), \\ \gamma_3 &= -(\omega_{31} - 2\dot{\phi} + \delta\omega_{31}),\end{aligned}$$

and

$$\begin{aligned}\delta\omega_{31} = {} & \Omega_{12}^2\left(\frac{1}{\dot{\phi} - \omega_{32}} + \frac{1}{3\dot{\phi} - \omega_{32}}\right) \\ & + \Omega_{23}^2\left(\frac{1}{\dot{\phi} - \omega_{21}} + \frac{1}{3\dot{\phi} - \omega_{21}}\right) \\ = {} & |\mu_{12}E_p/2\hbar|^2\left(\frac{1}{\dot{\phi} - \omega_{32}} + \frac{1}{3\dot{\phi} - \omega_{32}}\right) \\ & + |\mu_{23}E_p/2\hbar|^2\left(\frac{1}{\dot{\phi} - \omega_{21}} + \frac{1}{3\dot{\phi} - \omega_{21}}\right).\end{aligned}$$

5. Two-photon adiabatic following approximation

When the phase and amplitude of the field envelope vary slowly with respect to the magnitude of the two-photon rotation vector γ, e.g., $|\partial v(t)/\partial t|/|v(t)| \ll |\gamma_3(t)|$, where $v(t) = E_p^2(t)r_3(t)$, Eq. (3) can be solved approximately via an adiabatic following approximation [14], and the collective state of the Xe atoms can be expressed as

$$\begin{aligned}r_1 &= \pm\gamma_1/\left(\gamma_1^2 + \gamma_3^2\right)^{1/2}, \\ r_3 &= \pm\gamma_3/\left(\gamma_1^2 + \gamma_3^2\right)^{1/2}, \\ r_2 &= \dot{r}_3/\gamma_1 = \pm\frac{\gamma_1\dot{\gamma}_3 - \gamma_3\dot{\gamma}_1}{\left(\gamma_1^2 + \gamma_3^2\right)^{3/2}}.\end{aligned} \tag{4}$$

Given the initial condition $r = (0, 0, -1)$ and positive γ_3 the lower sign is appropriate. In this paper, the temporal incoherence of the NIKE laser induces large enough field fluctuations that the adiabatic following approximation condition is violated; however, the approximation is nonetheless a useful comparison. We further note that the adiabatic following approximation yields an effective modulation-instability gain that is asymmetric about the pump frequency. This is not, however, the cause of the small blue shift which appears in the $n_2(\dot{\phi})$ nonlinear response simulations; see Sec. IV.

6. Polarization

The total polarization is given by $\mathbf{P}(\mathbf{r}, t) = N\langle\hat{\boldsymbol{\mu}}\rangle = NTr(\rho\hat{\boldsymbol{\mu}}) = N(\langle 2|\hat{\boldsymbol{\mu}}|1\rangle\rho_{12} + \langle 3|\hat{\boldsymbol{\mu}}|2\rangle\rho_{23} + \text{c.c.})$ whose component along the linearly polarized real field of magnitude $E(\mathbf{r}, t) = |E_p(\mathbf{r}, t)|\cos[\phi(\mathbf{r}, t)]$ can be written as

$$\begin{aligned}P = {} & N(\mu_{12}\sigma_{12}(\phi)\exp(i\phi) + \mu_{12}\sigma_{12}(3\phi)\exp(3i\phi) \\ & + \mu_{23}\sigma_{23}(\phi)\exp(i\phi) + \mu_{23}\sigma_{23}(3\phi)\exp(3i\phi)) + \text{c.c.}\end{aligned}$$

The third-harmonic polarization component is included for completeness in this expression, but is neglected in the remainder of the discussion and in the simulations.

The envelopes $\sigma_{12}(n\phi)$ and $\sigma_{23}(n\phi)$ are well approximated by their adiabatic solutions in Eq. (A2b) because the respective detunings $|\omega_{21} - n\dot{\phi}|$ and $|\omega_{32} - n\dot{\phi}|$ that appear in $\dot{\sigma}_{12}(n\phi)$ and $\dot{\sigma}_{23}(n\phi)$ [see Eq. (A1)] far exceed the damping terms γ_N and γ_L or any spectral components in $\sigma_{12}(n\phi)$ and $\sigma_{23}(n\phi)$. Applying these results, ignoring the small damping terms $\gamma_{N,L}$, using $\Omega_{mn}^{\pm} = \mu_{mn}|E_p|/2\hbar$, then writing $\sigma_{33}(0\phi) \simeq (1 + r_3)/2$, $\sigma_{11}(0\phi) \simeq (1 - r_3)/2$, $\sigma_{13}(2\phi) = (r_1 - ir_2)/2$, we obtain the polarization associated with the two-photon vector model:

$$\begin{aligned}P/N \simeq {} & -\mu_{21}(\dot{\phi} - \omega_{21})^{-1}(\Omega_{12}^{+}\sigma_{11}(0\phi) \\ & + \Omega_{32}^{-}\sigma_{13}(2\phi))\exp(i\phi) + \mu_{32}(\dot{\phi} - \omega_{32})^{-1}(\Omega_{23}^{+}\sigma_{33}(0\phi) \\ & + \Omega_{21}^{-}\sigma_{13}(2\phi))\exp(i\phi) + \text{c.c.},\end{aligned} \tag{5a}$$

which becomes

$$\begin{aligned}P/N \simeq = {} & -(2\hbar)^{-1}\begin{pmatrix}\mu_{12}^2(\dot{\phi} - \omega_{21})^{-1}(1 - r_3) \\ -\mu_{23}^2(\dot{\phi} - \omega_{32})^{-1}(1 + r_3)\end{pmatrix}|E_p|\cos(\phi) \\ & - (2\hbar)^{-1}\mu_{12}\mu_{23}\begin{pmatrix}(\dot{\phi} - \omega_{21})^{-1} \\ -(\dot{\phi} - \omega_{32})^{-1}\end{pmatrix} \\ & \times |E_p|\begin{pmatrix}r_1\cos(\phi) \\ +r_2\sin(\phi)\end{pmatrix},\end{aligned} \tag{5b}$$

where we have defined the matrix elements $\mu_{12} = \mu_{21}$ and $\mu_{23} = \mu_{32}$ to be real, and ignored all even harmonic terms except $\sigma_{13}(2\phi)$. Using the two-photon adiabatic following approximation of Eq. (4) and neglecting the small damping

term $r_2 \propto \dot{\gamma}_1\,,\ \dot{\gamma}_3$, we obtain

$$P/N \simeq -(2\hbar)^{-1}\left(\gamma_1^2+\gamma_3^2\right)^{-1/2} \times \begin{pmatrix} \mu_{12}^2(\dot{\phi}-\omega_{21})^{-1}\left[\left(\gamma_1^2+\gamma_3^2\right)^{1/2}+\gamma_3\right] \\ -\mu_{23}^2(\dot{\phi}-\omega_{32})^{-1}\left[\left(\gamma_1^2+\gamma_3^2\right)^{1/2}-\gamma_3\right] \\ -\mu_{12}\mu_{23}\gamma_1((\dot{\phi}-\omega_{21})^{-1}-(\dot{\phi}-\omega_{32})^{-1}) \end{pmatrix} \times |E_p|\cos(\phi). \tag{5c}$$

In the small field limit where $\gamma_3 \gg \gamma_1$, this reduces to

$$P/N \approx \left(-\frac{\mu_{12}^2}{(\dot{\phi}-\omega_{21})\hbar} - |E_p|^2\frac{\mu_{12}^2\mu_{23}^2}{8\hbar^3} \times \left(\frac{1}{\dot{\phi}-\omega_{21}}-\frac{1}{\dot{\phi}-\omega_{32}}\right)^2\left(\frac{1}{2\dot{\phi}-\omega_{31}}\right)\right)|E_p|\cos(\phi). \tag{5d}$$

The polarization has the usual linear, dc terms as well as the nonlinear terms at the laser frequency.

From (5d), we obtain the following expression for the nonlinear refractive index:

$$\tilde{n}_2(\dot{\phi}) = \frac{N\mu_{12}^2\mu_{23}^2}{4\varepsilon_0 n_0\hbar^3(\omega_{31}-2\dot{\phi})(\omega_{21}-\dot{\phi})^2}, \tag{6}$$

where

$$P_{NL,p}(t) = \{2\varepsilon_0 n_0\tilde{n}_2[\dot{\phi}(t)]|E_p(t)|^2\}E_p(t), \tag{7}$$

$$E(t) = (1/2)E_p(t)\exp(-i\omega_0 t) + \text{c.c.} = |E_p(t)|\cos[\phi(t)], \tag{8a}$$

and

$$P_{NL}(t) = (1/2)P_{NL,p}(t)\exp(-i\omega_0 t) + \text{c.c.} \tag{8b}$$

Equations (6) and (7) represent the delayed Kerr response. The response time to an instantaneously switched-on intensity would be approximately the inverse of the smallest detuning factor. In Xe at 248 nm, this would be ~5 THz, corresponding to an ~2 ps delay time, which is much longer than the fs time scale of the linear response. The narrow-band limit of Eq. (6), i.e.,

$$\tilde{n}_2(\omega_0) = \frac{N\mu_{12}^2\mu_{23}^2}{4\varepsilon_0 n_0\hbar^3(\omega_{31}-2\omega_0)(\omega_{21}-\omega_0)^2},$$

can be obtained alternatively by expanding the density-matrix elements in powers of the field amplitude; see Ref. [5]. This will be referred to as the instantaneous Kerr response, or the steady-state case.

This result is obtained from the first-harmonic term of the nonlinear polarization and is consistent with the nonlinear index derived in Refs. [3,15], according to $\tilde{n}_2 = (1/2)\tilde{n}_{2,\text{alt}} = (1/8\pi)\tilde{n}_{2,\text{alt,cgs}}$, where $\tilde{n}_{2,\text{alt}}$ is defined according to $\varepsilon = (n_0+\tilde{n}_{2,\text{alt}}\langle E_p{}^2\rangle)^2 - 1 = (n_0+2\tilde{n}_2|E_p|^2)^2 - 1$, where the time-averaged field magnitude $\langle E_p{}^2\rangle = |E_p|^2/2$ and the subscript "cgs" refers to cgs units. We note that it has been derived in the small field limit under the two-photon adiabatic following approximation.

In the more general case, i.e., Eq. (5b), the nonlinear polarization $P_{NL}(t) = (1/2)P_{NL,p}(t)\exp(-i\omega_0 t) + \text{c.c.}$ can be expressed as shown below (see Appendix A for a discussion of the additional intermediate levels):

$$P_{NL,p}(t)/E_p(t) = (N/2\hbar)(\mu_{12}(\omega_{21}-\dot{\phi}-i\gamma_N)^{-1}[\mu_{23}\rho_Z - \mu_{12}(1+r_3)] - \mu_{23}(\omega_{32}-\dot{\phi}-i\,\gamma_L)^{-1}[\mu_{23}(1+r_3)+\mu_{12}\rho_Z]),$$

where $\rho_Z = 2\sigma_{13}(2\phi)^* = (r_1+ir_2)$ and Eq. (3) gives

$$\begin{aligned} d\rho_Z/dt &= i\gamma_3\rho_Z - i\gamma_1 r_3, \\ dr_3/dt &= \gamma_1 r_2 = i\gamma_1(\rho_Z^*-\rho_Z)/2 = i\gamma_1\rho_Z^*/2 + \text{c.c.}, \\ \gamma_1 &= \Omega_{12}\Omega_{23}\left(\frac{1}{\omega_{21}-\dot{\phi}}-\frac{1}{\omega_{32}-\dot{\phi}}\right) \\ &= \frac{\mu_{12}\mu_{23}}{\hbar^2}|E_p/2|^2\left(\frac{1}{\omega_{21}-\dot{\phi}}-\frac{1}{\omega_{32}-\dot{\phi}}\right), \\ \gamma_3 &= -(\omega_{31}-2\dot{\phi}+\delta\omega_{31}) \approx -(\omega_{31}-2\dot{\phi}). \end{aligned}$$

We note that the $(1-r_3)$ factor in Eq. (5b) has been rewritten as $2-(1+r_3)$. The first term represents the contribution to the linear index of refraction (approximately $\delta n_0 \sim 5\times10^{-4}$) and has been eliminated in order to yield the expression for $P_{NL,p}(t)$.

Alternatively, we can write the nonlinear polarization as

$$\begin{aligned} P_{NL,p}(t)/E_p(t) &= (N/2\hbar)(\mu_{12}(\omega_{21}-\dot{\phi}-i\gamma_N)^{-1}(\mu_{23}\rho_L) \\ &\quad - \mu_{23}(\omega_{32}-\dot{\phi}-i\,\gamma_L)^{-1}(\mu_{12}\rho_L))\frac{E_p^*(t)}{E_p(t)} \\ &\quad + (N/2\hbar)(\mu_{12}(\omega_{21}-\dot{\phi}-i\gamma_N)^{-1}[-\mu_{12}(1+r_3)] \\ &\quad - \mu_{23}(\omega_{32}-\dot{\phi}-i\,\gamma_L)^{-1}[\mu_{23}(1+r_3)]), \end{aligned} \tag{9}$$

where $\rho_L = (r_1+ir_2)\exp[2i\omega_0 t - 2i\phi(t)]$, and

$$\begin{aligned} d\rho_L/dt &= i\gamma_3'\rho_L - i\gamma_1' r_3, \\ dr_3/dt &= i\gamma_1'\rho_L^*/2 + \text{c.c.} = \text{Im}[(\gamma_1')^*\rho_L], \\ \gamma_1' &= \frac{\mu_{12}\mu_{23}}{\hbar^2}(E_p/2)^2\left(\frac{1}{\omega_{21}-\omega_0}-\frac{1}{\omega_{32}-\omega_0}\right), \\ \gamma_3' &= -(\omega_{31}-2\omega_0+\delta\omega_{31}) \approx -(\omega_{31}-2\omega_0). \end{aligned} \tag{10}$$

This latter form is preferable from a numerical standpoint because the instantaneous frequency $\dot{\phi}$ of a temporally incoherent laser tends to fluctuate wildly over short time scales, i.e., a much higher temporal resolution is required to resolve ρ_Z than to resolve ρ_L.

In the case of negligible population redistribution, Eq. (10) can be expressed by a single, driven harmonic-oscillator equation given by

$$(\partial/\partial t - i\gamma_3')\rho_L = i\gamma_1' \tag{11}$$

and solved exactly, i.e.,

$$\rho_L(t) = \rho_L(t_0)\exp\left(i\int_{t_0}^{t}\gamma_3'(t')dt'\right) + \int_{t_0}^{t}dt''i\gamma_1'(t'')\exp\left(i\int_{t''}^{t}\gamma_3'(t')dt'\right).$$

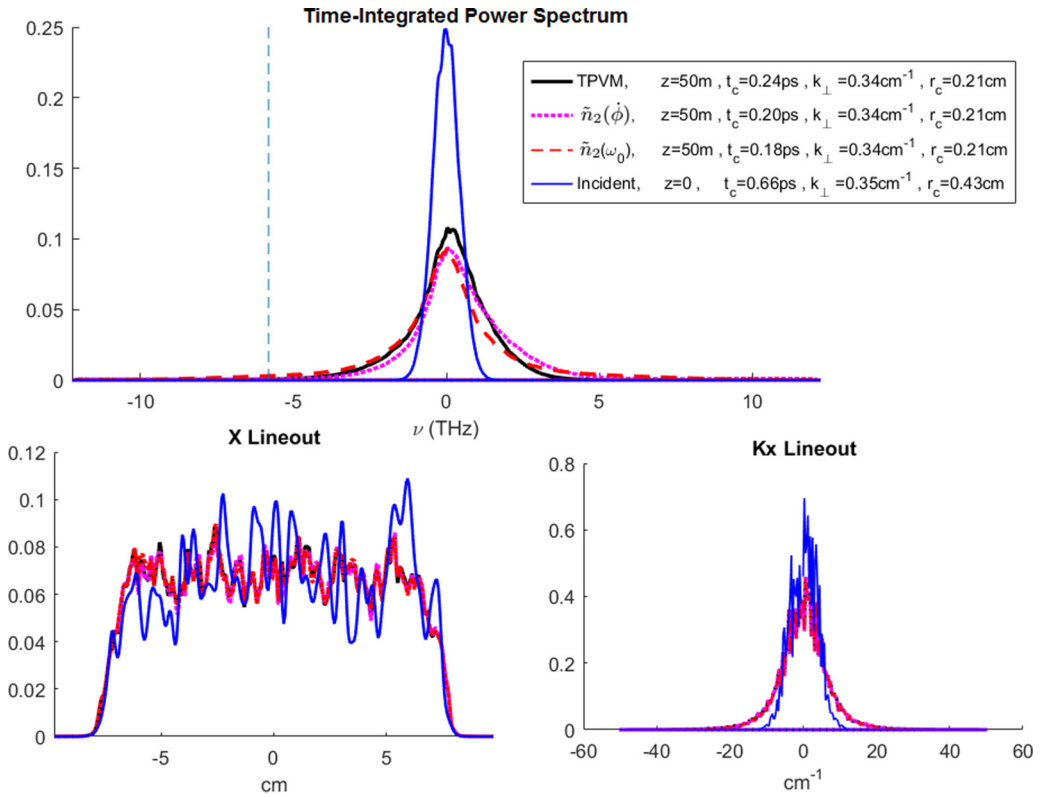

FIG. 3. Propagation of a 30 XDL (times diffraction limit) temporally and spatially incoherent KrF laser beam through 50 m of 200 mbar Xe gas; see Table I. (a) Total (time-integrated) power spectrum. (b) Axial lineout of near-field beam profile. (c) Axial lineout of far-field beam profile, modeled via the two-photon vector model (TPVM) using either Eqs. (10) or (11), the delayed Kerr response $\tilde{n}_2(\dot{\phi})$, see Eqs. (6) and (7), and the steady-state response $\tilde{n}_2(\omega_0)$. Properties of the incident light ($z = 0$) are indicated in black.

This solution can be evaluated more simply in frequency space, i.e., $\tilde{\rho}_L = i\tilde{\gamma}_1'/(i\omega - i\gamma_3')$.

Equations (9)–(11) are the working equations for all TPVM simulations.

III. NUMERICAL TECHNIQUES

The generalized nonlinear Schrödinger equation, see Eq. (1), is integrated along the propagation axis via a split-step method, where the diffraction term has been incorporated into the dispersive propagator and where calculation of the nonlinear propagator is parallelizable.

The nonlinear polarization of Xe gas according to the two-photon vector model can be calculated most generally via numerical time integration of the coupled first-order equations dr_3/dt and $d\rho_L/dt$ in Eq. (10) according to a straightforward iterative scheme—or in the case of negligible population redistribution Eq. (11). In the latter case, we opt for the straightforward frequency domain solution discussed above, which is an order of magnitude faster. Doing so requires that a small imaginary component be added to γ_3' to prevent divergent behavior.

The instantaneous frequency at time t is not required in our formulation of the two-photon vector model, see Eqs. (9)–(11), but it can be calculated by taking the derivative of the phase of the electric-field envelope having accounted for 2π phase jumps. Alternatively, it can be calculated by locating the spectral peak of the Fourier transform of the product of the field envelope and a narrow Gaussian centered about time t. The instantaneous frequency is used to calculate the nonlinear source term for the $\tilde{n}_2(\dot{\phi})$ response model given in Eqs. (6) and (7).

The input condition for the generalized nonlinear Schrödinger equation is discussed in Sec. II B of the paper. The filter function generating the top-hat beam shape is constructed from two hyperbolic tangent functions.

Guard bands are employed in frequency space to eliminate all energy above a frequency threshold (roughly 12 THz in Fig. 3), which is less than half of the maximum frequency in the simulation window, thereby avoiding aliasing across the periodic boundary imposed by the fast Fourier transform operation. The frequency threshold is set conservatively to ensure that the energy loss associated with the guard bands is not substantial. To simulate population redistribution can require enhanced time resolution, which corresponds to a wider frequency window. Regardless, the same frequency guard bands are applied to the electric field after each propagation step in order to eliminate any high-frequency artifacts which arise from the numerical integration of the coherence term.

Any error in the numerical integration especially for a longer pulse can slightly violate the energy conservation condition $\int_{-T/2}^{T/2} |\hat{E}(t,x,y)|^2 r_2(t,x,y)dt = 0$, which is valid in the limit that $\Gamma_c T \ll 1$. To address this concern, r_2 is shifted accordingly upward or downward by a very small,

TABLE I. Simulation parameters for Figs. 3 and 4.

KrF beam/Xe properties	
Peak power	33 GW
Beam size	15 cm × 15 cm
Transverse coherence length	0.5 cm (i.e., XDL = 30[a])
Pulse length	>10 ps
Pulse temporal shape	Gaussian
Pulse transverse spatial shape	Flat-top beam with smoothed edges
Linewidth	1 THz
Detuning of $2\omega_0$ from two-photon resonance	11.9 THz
Nonlinear refractive index at ω_0[b]	-190×10^{-19} cm^2/W
Group-velocity dispersion coefficient	8.2×10^{-6} ps^2/cm

[a]The times diffraction limit (XDL) is often denoted elsewhere in the literature as M_x^2.
[b]Reference [4]. This value may be a 15%–20% overestimate; see Ref. [3].

smooth plateau of the pulse width T after each integration step. The necessary resolution along the propagation axis can be reduced by splitting the growth or decay part of the nonlinear propagator into smaller, energy-conserving steps, i.e., $\exp(\alpha r_2 \Delta z) \approx \sum_n (\sqrt{1+\alpha r_2 \Delta z/n})^{2n}$. Grid resolution requirements in both vector spaces are imposed as well.

IV. NUMERICAL RESULTS

The propagation of a temporally and spatially incoherent KrF laser beam through a chamber of 200 mbar Xe gas is simulated in this section. The simulation parameters are listed in Table I and correspond to the incident beam in Ref. [13].

Figures 3 and 4 are simulated according to Eq. (1). In Fig. 3, the nonlinear polarization for the TPVM is given by Eq. (9) and is determined by solving Eq. (11) in frequency space; to determine it according to Eq. (10) yields the same result because population inversion is small. The nonlinear polarization in the second model in Fig. 3 is determined according to Eqs. (6) and (7), and the nonlinear polarization in the third model in Fig. 3 is the instantaneous Kerr nonlinearity $\tilde{n}_2(\omega_0)$, also referred to here as the steady-state solution. Each data point in Fig. 4 is simulated also according to Eq. (1), for its own, noise-generated incident beam with the specified times diffraction limit. To clarify the physical behavior, the nonlinear polarization used in Fig. 4 has been determined according to the steady-state solution as opposed to Eqs. (9) and (11); the trends and conclusions, however, are the same.

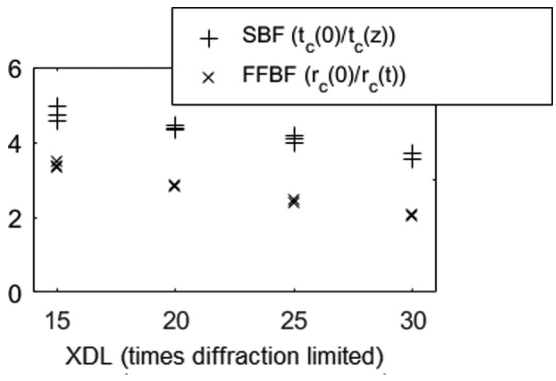

FIG. 4. Spectral broadening factor and far-field broadening factor are plotted as a function of the times diffraction limit (XDL), for propagation of a temporally and spatially incoherent KrF laser beam through 50 m of 200 mbar Xe gas. To clarify the physics, the nonlinear polarization in this figure has been determined according to the steady-state model as opposed to Eqs. (9) and (11). All trends and conclusions, however, are the same.

We obtain the following results, in which the coherence time is estimated according to the expression $t_c = \int (P(\nu))^2 d\nu$, where $P(\nu)$ is the normalized total (time-integrated) power spectrum of the beam, i.e., $\int P(\nu) d\nu = 1$. This enables the calculation of a spectral broadening factor defined as $\mathrm{SBF} = t_c(0)/t_c(z)$, where z is the propagation distance. Similarly, to quantify the broadening of the far-field profile (whose shape is identical to the near-field transverse spatial frequency spectrum), we substitute it into the 2D spatial version of the t_c expression to calculate the near-field transverse coherence zone radius r_c; this gives the far-field broadening factor $\mathrm{FFBF} = r_c(0)/r_c(z)$. This factor is essentially unchanged if we use the 1D (along the x axis) spatial version of the t_c expression. The small broadening of the near-field profile itself can be estimated by the beam spread factor $\mathrm{BSF} = 1 + (k_\perp/k_0)z/D$, where $k_\perp/k_0$ is the beam spreading angle, $k_\perp$ is the spatial frequency version of r_c, and $D = 15$ cm is the beam width. The small beam spread (BSF ≈ 1.0005) arises in part due to the ISI beam divergence and in part due to the effects of the nonlinear far-field broadening.

The amount of spectral broadening seen in Fig. 3 for 50 m of 200 mbar Xe is comparable to that seen in Ref. [13] for beam propagation through a 100 m air path.

The transverse spatial behavior in Fig. 3 is independent of whether the nonlinearity is calculated according to the TPVM, delayed Kerr response $\tilde{n}_2(\dot{\phi})$, or steady-state response $\tilde{n}_2(\omega_0)$. The spectral behavior, however, is model dependent. The TPVM displays a reduction in high frequencies; its difference with respect to the delayed Kerr response $\tilde{n}_2(\dot{\phi})$ can be attributed to the large field fluctuations, which render inaccurate the step used to obtain Eq. (5c) (in which the adiabatic following approximation was applied and the $\dot{\gamma}_i$ term was neglected).

Since the simulations are only for a 30 times-diffraction-limited beam (due to computational constraints), it is useful to consider how the propagation properties of a 75 times-diffraction-limited beam will differ; see Fig. 4. The spectral broadening factor (SBF) is reduced as XDL increases, as is the far-field broadening factor (FFBF). These effects can be attributed to the phase mismatch of the 3D wave vectors involved in four wave mixing or, equivalently, the interruption of amplification paths. For a smaller spot size, the beam spreading factor (BSF) can become significant and increase with XDL, such that the SBF and FFBF decrease more significantly with XDL than in Fig. 4 and roughly in proportion to $(1 + \mathrm{XDL}/a)^{-2}$, where a is some constant. The small beam spread (BSF ≈ 1.0005) is due to the effects of far-field broadening and is roughly an order of magnitude larger than it would be due to ISI beam divergence alone.

It is expected (for the parameters in Table I) that at 75 times diffraction limit the SBF will be roughly 2, and that the FFBF

will be less than that; see Fig. 4. It must be noted, however, that the nonlinearity may be overestimated by 15%–20%; see Table I. The SBF is larger than the FFBF in Fig. 4, which we have seen in simulations is in part due to the four wave mixing phase mismatch mentioned above, but can be mostly attributed to the positive group-velocity dispersion coefficient, which in a negative-n_2 medium sharpens the pulse in time, thereby increasing the rate of spectral broadening.

V. DISCUSSION

We have shown that propagation of the KrF NIKE laser output beams through Xe gas may be an effective way of increasing the laser bandwidth beyond that which can be achieved via SRRS in air or nitrogen [13]. The near-field beam spreading factor is negligible in both approaches and, while the far-field broadening factor is signifcant, it is smaller than the spectral broadening factor, which has been enhanced by group-velocity dispersion. In both approaches, far-field broadening may limit the propagation distance and thus the spectral broadening that can be achieved. Xenon has the advantage that it responds almost instantaneously (∼1 ps) to the incident pulse, while SRRS in air or nitrogen requires buildup times ∼100 ps determined by the ∼3 GHz pressure-broadened rotational linewidths. However, the simulations in Ref. [13] show that, just beyond the peak of the ∼400 ps pulse, the time-resolved spectra are significantly broader than the time-integrated spectra; this suggests that the SRRS would be more effective for longer (ns) pulses. The best way to maximize the spectral broadening, while limiting the degradation of the far-field beam profile, may be propagation through a medium containing both air and Xe to combine the two approaches.

VI. CONCLUSION

The nonlinear response of Xe gas to chaotic non-steady-state, near-resonance light has been modeled using a two-photon vector model. The propagation of the KrF NIKE laser light through 200 mbar Xe has been simulated, and a dependence of the spectral broadening and beam profile degradation on the times diffraction limit is observed and discussed. The results of the TPVM are compared with those of a delayed response model and an instantaneous response model. We conclude that propagation of the KrF NIKE laser output beams through Xe may be an effective way of increasing the laser bandwidth, thereby suppressing the laser-plasma instabilities.

ACKNOWLEDGMENTS

We acknowledge funding by the US Department of Energy (DOE) and the National Nuclear Security Administration (NNSA).

APPENDIX A

1. Parameters

For a 248.4 nm laser pulse propagating through an atomic Xe gas, the two-photon excited state is the Xe $6p[1/2]0$ state, and a classical collisional model predicts an elastic collision rate of $\gamma_c \sim 4P\pi r_{\rm Xe}^2\sqrt{2/m_{\rm Xe}kT} = 2.4$ GHz × (P/bar), where P is the pressure of the Xe gas, T is the gas temperature, and $m_{\rm Xe}$ and $r_{\rm Xe}$ are the mass and van der Waals radius of an individual Xe molecule. We estimate the spontaneous emission rates as $A_{32} = |\mu_{32}|^2\omega_{32}^3/(3\pi\varepsilon_0\hbar c^3) \approx 40$ MHz and $A_{21} = |\mu_{21}|^2\omega_{21}^3/(3\pi\varepsilon_0\hbar c^3) \approx 5$ GHz (see Ref. [16]). The FWHM of the two-photon absorption spectrum given a laser linewidth $\Delta\omega_L = 2.9$ GHz is measured to be $\Delta\nu_{\rm FWHM} = 4.6 + 3.5(P/\text{bar})$ GHz $\approx \sqrt{\Delta\nu_L^2 + \Delta\nu_D^2} + \gamma_c$ (see Ref. [8]), where the Doppler broadening linewidth $\Delta\nu_D = 2\nu_0(2k_BT\ \ln 2/m_{\rm Xe})^{1/2}/c \approx 1.3$ GHz and the elastic collision rate $\gamma_c \sim 4P\pi r_{\rm Xe}^2\sqrt{2/m_{\rm Xe}kT} = 2.4$ GHz × (P/bar) are in agreement with the experimental result. The radiative rate of the excited Xe state is measured to be ∼30 MHz (see Ref. [17]), which is consistent with the limiting spontaneous emission rate of 40 MHz. For a KrF NIKE pulse, the 600 ps short pulses and 4 ns long pulses correspond to a frequency scale 1.7 GHz and 0.3 GHz, respectively. The elastic collision rate at 200 mbar is 0.5 GHz and the inelastic collision rate is presumably at least an order of magnitude smaller.

2. Density-matrix equations

The density-matrix equations given in Eq. (1) can be rewritten for integer $s \in (-3, -2, \ldots, 3)$ and shown below:

$$
\begin{aligned}
\dot\sigma_{11}(s\phi) &= (-is\dot\phi - \Gamma_o)\sigma_{11}(s\phi) + \delta_s\Gamma_0\rho_{11}^{eq} \\
&\quad + a\Gamma_I\left[\sigma_{22}(s\phi) - \delta_s\rho_{22}^{eq}\right] + ab\Gamma_c\left[\sigma_{33}(s\phi) - \delta_s\rho_{33}^{eq}\right] \\
&\quad + \sum_{\pm} i(\Omega_{12}^{\pm}\sigma_{21}[\phi(s\mp 1)] - \Omega_{21}^{\pm}\sigma_{12}[\phi(s\mp 1)]), \\
\dot\sigma_{22}(s\phi) &= (-is\dot\phi - \Gamma_I)\sigma_{22}(s\phi) + \delta_s\Gamma_I\rho_{22}^{eq} \\
&\quad + a(1-b)\Gamma_c\left[\sigma_{33}(s\phi) - \delta_s\rho_{33}^{eq}\right] \\
&\quad + \sum_{\pm} i(\Omega_{21}^{\pm}\sigma_{12}[\phi(s\mp 1)] - \Omega_{12}^{\pm}\sigma_{21}[\phi(s\mp 1)] \\
&\quad + \Omega_{23}^{\pm}\sigma_{32}[\phi(s\mp 1)] - \Omega_{32}^{\pm}\sigma_{23}[\phi(s\mp 1)]), \\
\dot\sigma_{33}(s\phi) &= (-is\dot\phi - \Gamma_c)\sigma_{33}(s\phi) + \delta_s\Gamma_c\rho_{33}^{eq} \\
&\quad + \sum_{\pm} i(\Omega_{32}^{\pm}\sigma_{23}[\phi(s\mp 1)] - \Omega_{23}^{\pm}\sigma_{32}[\phi(s\mp 1)]), \\
\dot\sigma_{12}(s\phi) &= (-is\dot\phi + i\,\omega_{21} - \ \gamma_N)\sigma_{12}(s\phi) \\
&\quad + \sum_{\pm} i(\Omega_{12}^{\pm}\{\sigma_{22}[\phi(s\mp 1)] - \sigma_{11}[\phi(s\mp 1)]\} \\
&\quad - \Omega_{32}^{\pm}\sigma_{13}[\phi(s\mp 1)]), \\
\dot\sigma_{13}(s\phi) &= (-is\dot\phi + i\,\omega_{31} - \ \gamma_c)\sigma_{13}(s\phi) \\
&\quad + \sum_{\pm} i\,(\Omega_{12}^{\pm}\sigma_{23}[\phi(s\mp 1)] - \Omega_{23}^{\pm}\sigma_{12}[\phi(s\mp 1)]), \\
\dot\sigma_{23}(s\phi) &= (-is\dot\phi + i\,\omega_{32} - \ \gamma_L)\sigma_{23}(s\phi) \\
&\quad + \sum_{\pm} i\,(\Omega_{23}^{\pm}\{\sigma_{33}[\phi(s\mp 1)] - \sigma_{22}[\phi(s\mp 1)]\} \\
&\quad + \Omega_{21}^{\pm}\sigma_{13}[\phi(s\mp 1)]).
\end{aligned}
\tag{A1}
$$

3. Two-photon vector model

On a time scale that is much longer than the inverse of the detuning $2\pi/\Delta \sim 0.2$ ps, where $\Delta = (2\omega_0 - \omega_{31})/2$, the off-diagonal density-matrix elements will be significantly driven only near the various harmonics of the laser frequency. This means the components $\sigma_{mn}(s\phi)$ can be taken to be slowly varying in time, i.e., $|\dot{\sigma}_{mn}(s\phi)|/|\omega_0\sigma_{mn}(s\phi)| \sim |(\omega_{31} - 2\dot{\phi})|/\omega_0 = |\Delta|/\omega_0 \ll 1$. In the given case where each one-photon transition is off resonance, this allows us to take, to zeroth order in Δ/ω_0, $|\dot{\sigma}_{12}(s\phi)| \ll |(-is\dot{\phi} + i\,\omega_{21} - \gamma_N)\sigma_{12}(s\phi)|, |\dot{\sigma}_{23}(s\phi)| \ll |(-is\dot{\phi} + i\,\omega_{32} - \gamma_L)\sigma_{23}(s\phi)|$. In this case it is also reasonable to neglect the population of the intermediate state σ_{22} because it is driven off resonance and is to second order in the field. Since the time scale of the pulse may be comparable to or shorter than the average elastic collision time, there are non-negligible transient components of ρ_{12} and ρ_{23} as well. However, these components are nonresonant with the harmonics of the laser frequency and thus represent only a contribution to the linear response.

The near-resonance components $\sigma_{11}(0), \sigma_{33}(0), \sigma_{13}(2\phi)$ can be identified as the ones which drive other elements and contribute significantly to the polarization field. Simplifying the expression and redefining the eigenstates such that the dipole moments $\mu_{12} = \mu_{21}$ and $\mu_{23} = \mu_{32}$ are real, we obtain, for linear polarization,

$$\Omega_{12}^{+\,*} = [\Omega_{12}^{-}] = \Omega_{12}^{+} \to \Omega_{12}, \quad \Omega_{23}^{+} \to \Omega_{23} \tag{A2a}$$

and

$$\begin{aligned}
\sigma_{12}(s\phi) &\approx (s\dot{\phi} - \omega_{21} - i\gamma_N)^{-1} \sum_{\pm} (\Omega_{12}\{\sigma_{11}[\phi(s \mp 1)]\} \\
&\quad + \Omega_{32}\sigma_{13}[\phi(s \mp 1)]), \\
\sigma_{23}(s\phi) &\approx (-s\dot{\phi} + \omega_{32} + i\gamma_L)^{-1} \sum_{\pm} (\Omega_{23}\sigma_{33}[\phi(s \mp 1)] \\
&\quad + \Omega_{21}\sigma_{13}[\phi(s \mp 1)]),
\end{aligned}$$

$$\begin{aligned}
\dot{\sigma}_{13}(2\phi) &= A\sigma_{13}(2\phi) + B\sigma_{11}(0\phi) + C\sigma_{33}(0\phi), \\
\dot{\sigma}_{11}(0\phi) &= E\sigma_{13}(2\phi) + \text{c.c.} + F\sigma_{11}(0\phi) + \text{c.c.} \\
&\quad + G\sigma_{33}(0\phi) + \text{c.c.} + H, \\
\dot{\sigma}_{33}(0\phi) &= J\sigma_{13}(2\phi) + \text{c.c.} + L\sigma_{33}(0\phi) + \text{c.c.} + M,
\end{aligned} \tag{A2b}$$

where $E = B$ and $J = C$ from Eq. (A2a), and

$$\begin{aligned}
A &= [i(\omega_{31} - 2\dot{\phi}) - \gamma_c] \\
&\quad - \Omega_{12}^2\left(\frac{1}{i\dot{\phi} - i\,\omega_{32} + \gamma_L} + \frac{1}{3i\dot{\phi} - i\,\omega_{32} + \gamma_L}\right) \\
&\quad - \Omega_{23}^2\left(\frac{1}{i\dot{\phi} - i\,\omega_{21} + \gamma_N} + \frac{1}{3i\dot{\phi} - i\,\omega_{21} + \gamma_N}\right), \\
B &= -\Omega_{12}\Omega_{23}(i\dot{\phi} - i\,\omega_{21} + \gamma_N)^{-1}, \\
C &= -\Omega_{12}\Omega_{23}(i\dot{\phi} - i\,\omega_{32} + \gamma_L)^{-1}, \\
E &= -\Omega_{12}\Omega_{23}(i\dot{\phi} - i\,\omega_{21} + \gamma_N)^{-1} = B, \\
F &= -\Gamma_o/2 - \Omega_{12}^2(i\dot{\phi} - i\,\omega_{21} + \gamma_N)^{-1} \\
&\quad - \Omega_{12}^2(-i\dot{\phi} - i\,\omega_{21} + \gamma_N)^{-1}, \\
G &= +ab\Gamma_c/2, \\
H &= \Gamma_0\rho_{11}^{eq} - ab\Gamma_c\rho_{33}^{eq}, \\
J &= -\Omega_{12}\Omega_{23}(i\dot{\phi} - i\,\omega_{32} + \gamma_L)^{-1} = C, \\
L &= -\Gamma_c/2 - \Omega_{23}^2(i\dot{\phi} - i\,\omega_{32} + \gamma_L)^{-1} \\
&\quad - \Omega_{23}^2(-i\dot{\phi} - i\,\omega_{32} + \gamma_L)^{-1}, \\
M &= \Gamma_c\rho_{33}^{eq}.
\end{aligned}$$

Defining a real vector $r = (r_1, r_2, r_3)$ where $r_1 = \sigma_{13}(2\phi) + [\sigma_{13}(2\phi)]^*$, $r_2 = i(\sigma_{13}(2\phi) - [\sigma_{13}(2\phi)]^*)$, $r_3 = \sigma_{33}(0\phi) - \sigma_{11}(0\phi)$, we can rewrite Eq. (A2b) to zeroth order in Δ/ω_0 as

$$\begin{aligned}
\dot{r}_1 &= A(r_1 - ir_2)/2 + A^*[(r_1 - ir_2)/2]^* - \Omega_{12}\Omega_{23}\left[\frac{\gamma_N}{(\dot{\phi} - \omega_{21})^2 + \gamma_N^2}(1 - r_3) + \frac{\gamma_L}{(\dot{\phi} - \omega_{32})^2 + \gamma_L^2}(1 + r_3)\right], \\
\dot{r}_2 &= i(A(r_1 - ir_2)/2 - A^*[(r_1 - ir_2)/2]^*) - \Omega_{12}\Omega_{23}\left[\frac{\dot{\phi} - \omega_{21}}{(\dot{\phi} - \omega_{21})^2 + \gamma_N^2}(1 - r_3) + \frac{\dot{\phi} - \omega_{32}}{(\dot{\phi} - \omega_{32})^2 + \gamma_L^2}(1 + r_3)\right], \\
\dot{r}_3 &= -i\Omega_{12}\Omega_{23}\left(\frac{1}{\omega_{32} - \dot{\phi} + i\gamma_L} - \frac{1}{\omega_{21} - \dot{\phi} + i\gamma_N}\right)(r_1 - ir_2)/2 + \text{c.c.} \\
&\quad + \left[\Gamma_0/2 + \gamma_N\Omega_{12}^2\left(\frac{1}{(\dot{\phi} - \omega_{21})^2 + \gamma_N^2} + \frac{1}{(\dot{\phi} + \omega_{21})^2 + \gamma_N^2}\right)\right](1 - r_3) \\
&\quad + \left[-(1 + ab)\Gamma_c/2 - \gamma_L\Omega_{23}^2\left(\frac{1}{(\dot{\phi} - \omega_{32})^2 + \gamma_L^2} + \frac{1}{(\dot{\phi} + \omega_{32})^2 + \gamma_L^2}\right)\right](1 + r_3) + \left[\Gamma_c(1 + ab)\rho_{33}^{eq} - \Gamma_0\rho_{11}^{eq}\right],
\end{aligned} \tag{A3}$$

where we have made the replacements $\sigma_{13}(2\phi) = (r_1 - ir_2)/2$, $\sigma_{11}(0\phi) \simeq (1 - r_3)/2$, $\sigma_{33}(0\phi) \simeq (1 + r_3)/2$.

4. Polarization

Treatment of intermediate states

In the case of multiple intermediate levels, we can sum over states $|2\rangle$ to obtain the total polarization. According to energy of each intermediate state and its transition dipole moments, one can determine the fractional contribution of each state to the nonlinear index given in Eq. (7). However, treatment of multiple intermediate levels in the two-photon

vector model shouldn't be important for comparing simulations with future experiments (except in the case when population redistribution is significant). This is because the additive contribution of each intermediate state to the nonlinear index $\sim\mu_{12}\mu_{23}/(\omega_{21}-\omega_0)$ is of the same form as its contribution to the more general expression for the nonlinear polarization, see Eq. (10) and Eq. (5a), thereby producing a response that is representative of a two-photon transition with only one intermediate state.

APPENDIX B

Two-photon absorption rate

Solving Eq. (3) given the initial condition $r(t=0)=(0,0,-1)$ and a constant (or slowly varying in time) field amplitude and phase, i.e., $\dot{\gamma}/\gamma^2 \ll 1$, we obtain $r_3 = -1 + \gamma_1^2[1-\cos(t\sqrt{\gamma_1^2+\Delta^2})]/(\gamma_1^2+\Delta^2)$. We can then express the two-photon excited population ρ_{33} as $\rho_{33} \approx (1+r_3)/2 = \gamma_1^2\sin^2(t\sqrt{\gamma_1^2+\Delta^2}/2)/(\gamma_1^2+\Delta^2) \sim 10^{-9}$ for the average field intensity and detuning given in Table I. For long times, in the low-intensity limit, we express ρ_{33} as a function of frequency and obtain the following function which peaks at $\Delta=0$: $\rho_{33}(\Delta) \approx \frac{\gamma_1^2\sin^2(t\Delta/2)}{\Delta^2} = \frac{\pi\gamma_1^2 t}{2}[\frac{\sin^2(\Delta t/2)}{\pi(t/2)\Delta^2}]$. Applying the relation for the long time limit, we can recover the standard two-photon absorption rate $R_{2\gamma}$. The transition probability is given by $R_{2\gamma}t = \int[\lim_{(t/2)\to\infty}\rho_{33}(\Delta)]g(\Delta)d\Delta = (\pi\gamma_1^2 t/2)\int\delta(\Delta)g(\Delta)d\Delta$, from which we obtain $R_{2\gamma} = \pi\gamma_1^2 g(0)/2 = 2\pi g(0)(\Omega_{12}\Omega_{23})^2/(\omega_{21}-\dot{\phi})^2$, where $g(\Delta)$ is the energy density. After 50 m propagation according to the parameters in Table I, the energy density on resonance is given by $g(0) \sim 10^{-3}$ THz^{-1}. Hence a transition rate $R_{2\gamma} \sim$ kHz is obtained for a sufficiently slowly varying field amplitude and phase, i.e., $\dot{\gamma}/\gamma^2 \ll 1$.

[1] R. Betti and O. A. Hurricane, Inertial-confinement fusion with lasers, Nat. Phys. **12**, 435 (2016).

[2] S. Obenschain, R. Lehmberg, D. Kehne, F. Hegeler, M. Wolford, J. Sethian, J. Weaver, and M. Karasik, High-energy krypton fluoride lasers for inertial fusion, Appl. Opt. **54**, F103 (2015).

[3] R. H. Lehmberg, C. J. Pawley, A. V. Deniz, M. Klapisch, and Y. Leng, Two-photon resonantly-enhanced negative nonlinear refractive index in xenon at 248 nm, Opt. Commun. **121**, 78 (1995).

[4] E. T. J. Nibbering, G. Grillon, M. A. Franco, B. S. Prade, and A. Mysyrowicz, Determination of the inertial contribution to the nonlinear refractive index of air, N_2, and O_2 by use of unfocused high-intensity femtosecond laser pulses, JOSA B **14**, 650 (1997).

[5] R. H. Lehmberg, J. Reintjes, and R. C. Eckardt, Negative nonlinear susceptibility of cesium vapor around 1.06 μm, Phys. Rev. A **13**, 1095 (1976).

[6] D. Grischkowsky, M. M. T. Loy, and P. F. Liao, Adiabatic following model for two-photon transitions: Nonlinear mixing and pulse propagation, Phys. Rev. A **12**, 2514 (1975).

[7] D. Grischkowsky, Coherent excitation, incoherent excitation, and adiabatic states, Phys. Rev. A **14**, 802 (1976).

[8] W. Gornik *et al.*, Two-photon excitation of xenon atoms and dimers in the energy region of the 5 p 56 p configuration, J. Chem. Phys. **75**, 68 (1981).

[9] R. H. Lehmberg and S. P. Obenschain, Use of induced spatial incoherence for uniform illumination of laser fusion targets, Opt. Commun. **46**, 27 (1983).

[10] R. H. Lehmberg, A. J. Schmitt, and S. E. Bodner, Theory of induced spatial incoherence, J. Appl. Phys. **62**, 2680 (1987).

[11] T. Brabec and F. Krausz, Nonlinear Optical Pulse Propagation in the Single-Cycle Regime, Phys. Rev. Lett. **78**, 3282 (1997).

[12] T. R. Taha and M. I. Ablowitz, Analytical and numerical aspects of certain nonlinear evolution equations. II. Numerical, nonlinear Schrödinger equation, J. Comput. Phys. **55**, 203 (1984).

[13] J. Weaver, R. Lehmberg, S. Obenschain, D. Kehne, and M. Wolford, Spectral and far-field broadening due to stimulated rotational Raman scattering driven by the NIKE krypton fluoride laser, Appl. Opt. **56**, 8618 (2017).

[14] M. D. Crisp, Adiabatic-following approximation, Phys. Rev. A **8**, 2128 (1973).

[15] D. Grischkowsky and J. A. Armstrong, Self-defocusing of light by adiabatic following in rubidium vapor, Phys. Rev. A **6**, 1566 (1972).

[16] M. R. Junnarkar, R. Mahesh, and N. Uesugi, Near-two-photon-resonance short-pulse propagation in atomic xenon, *Optical Pulse and Beam Propagation* (International Society for Optics and Photonics, San Jose, CA, 1999), Vol. 3609.

[17] M. R. Bruce *et al.*, Radiative lifetimes and collisional deactivation of two-photon excited xenon in argon and xenon, J. Chem. Phys. **92**, 2917 (1990).